

# Preparation and Characterization of CuO/Clay Composite for Methyl Orange Photodegradation

Sumiati Side<sup>1</sup>, Suriati Eka Putri<sup>1,\*</sup>, Hasri<sup>1</sup>, and Abd Rahman<sup>2</sup>

<sup>1</sup>Chemistry Department, Mathematics and Natural Science Faculty, Universitas Negeri Makassar, Jalan Daeng Tata Raya Makassar, 90224, Indonesia

<sup>2</sup>Inorganic Chemistry, King Fahd University of Petroleum & Minerals, Academic Belt Road, Dhahran, 31261, Saudi Arabia

**Abstract.** This study reports on the preparation and characterizations of CuO/clay composite and its application for methyl orange (MO) photodegradation. The raw material of natural clay was obtained from Takalar District, South Sulawesi Province of Indonesia. CuO were incorporated in clay by impregnation method, with natural clay was intercalated using CMC before. The new composite was characterized by SEM, nitrogen adsorption-desorption measurements, and XRD. The results from SEM analysis revealed that there is a change in the surface morphology of the sample before and after impregnation, the clay becomes more porous and expands. XRD results show the CuO/clay composite has a monoclinic crystal structure. As for the sample surface area based on BET analysis using t-plot method, the surface area decreased after the CuO impregnated and the pore distribution using BJH analysis decrease, it indicates that CuO was successfully impregnated into the clay. The amount of CuO that was successfully impregnated into clay based on EDX analysis was 26.72%. The composite was successfully used as a photocatalyst in the MO degradation, showing a degradation ability of 85.84% with a composite mass of 500 mg with a contact time of 180 minutes.

## 1 Introduction

Synthetic dyes are frequently utilized in a variety of industries, particularly the textile industry. The majority of synthetic dyes are azo dyes, which have been found to have the potential to be genotoxic and carcinogenic [1]. Dyes in water can absorb most of the sunlight, thereby preventing the development of aquatic species and reducing dissolved oxygen [2]. The methyl orange (MO) dyes were investigated in this study. MO has an azo band (-N=N-) associated with two aromatic rings and is used for colouration in textile industries. The waste causes serious environmental pollution and if accumulated in the body causes deterioration of human health [3].

In order to lessen the environmental impact, dye removal or degradation from wastewater has been extensively explored. Different dyes have been effectively treated using a variety of physical, chemical, and biological techniques, including adsorption [4], ozonation [5,6], Fenton [7,8], photocatalysis [9,10], reductive degradation [11,12], microbial processes [3,13], and two or more combination techniques. However, these treatments also face other drawbacks in the treatment of experimental dye wastewater, such as a sluggish reaction rate to decolorize effluents, complicated chemistry, and metal ion sludge [14].

An emerging to conventional methods which has emerged as a green and promising technology is the

photocatalytic method due to the complete mineralization of organic pollutants by light irradiation [15]. Besides, this method is a quick, affordable, and simple to use for industrial-scale dye removal. The widely used metal oxides such as TiO<sub>2</sub> [16], Fe<sub>2</sub>O<sub>3</sub> [17], ZnO [18], NiO [19], and so on. The photocatalytic efficiency, which is based on the complete UV spectrum, is quite low and unstable despite their comparatively high band gap energies. In addition, the copper oxide (CuO) are widely used in the degradation process as an important p-type semiconductor. The narrow band gap s of CuO of 1.2-1.7 eV, absorbs visible light to generate electron-hole pairs (e<sup>-</sup> -h<sup>+</sup>) with enough life-time to let chemical reaction occur [20]. Compared to titanium oxide (TiO<sub>2</sub>), CuO is low cost, abundant, and economical material with short reaction time under normal conditions which is favorable in the synthesis of green chemistry [14].

There are some reports in the literature on the synthesis and application of CuO as catalyst in the photodegradation process on different azo dyes wastewater. Ramesh [14] reported CuO as an efficient photocatalyst for the degradation of azo dyes in wastewater, the results show that the highest degradation achieved was 67.8% and 66.3% for Reactive Black 5 dye and Acid Yellow-23 dye from aqueous solution at 5 h illumination. Mendoza et al. [2] reported that CuO supported on ZnO complete degradation of MO for 30 mins with catalyst quantity of

\* Corresponding author: [ekaputri\\_chem@unm.ac.id](mailto:ekaputri_chem@unm.ac.id)

150 mg and dye solution tested of 450 mL of 20 ppm. The results obtained are higher than using only CuO.

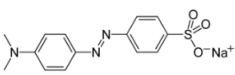
Recent studies showed that combining CuO semiconductors with supporting materials can increase the activities of semiconductor. Among the catalyst supports that have been used are zeolites [20], gamma alumina [21], and carbon nanotube [22]. The use of this porous material as a support catalyst due to its unique properties including size, charge, ion exchange, large surface area, and shape selectivity, is a good candidate for supporting semiconductors into it. In addition, clay which is a natural porous mineral which is quite abundant has also been used as a catalyst support for the dyes degradation. Sohrabnezhad and Takas [23] intercalated clay with CuO for Methylene Blue (MB) dye degradation, after 60 minutes, the photocatalyst showed 94% removal efficiency for MB dye under visible light. To the best of our knowledge, there is no report on photodegradation of MO dyes using CuO/Clay composites. In this study CuO/clay composites synthesized by wet impregnation method were used for the degradation of MO dyes in the absence of H<sub>2</sub>O<sub>2</sub>.

## 2 Material and Method

### 2.1 Materials

Natural clay was obtained from Takalar District, South Sulawesi Province of Indonesia (the characteristic was shown in Table 1), Copper(II)sulphate (CuSO<sub>4</sub>.5H<sub>2</sub>O), surfactant carboxymethyl cellulose (CMC), and ethanol 96% were purchased from Sigma-Aldrich. Analytical grade materials were all employed in this experiment without additional purification. All the trials utilized deionized water. The target compound, MO, is an azo dye, and Table 1 displays its chemical composition.

**Table 1.** The characteristic of clay and the chemical structure of MO

<b>Natural clay</b>	
Chemical analysis (using XRF; %wt)	SiO <sub>2</sub> : 65.00; Al <sub>2</sub> O <sub>3</sub> : 9.37; Fe <sub>2</sub> O <sub>3</sub> : 14.84; K <sub>2</sub> O: 4.51; CaO: 3.04; TiO <sub>2</sub> : 1.68; MnO: 0.41; P <sub>2</sub> O <sub>5</sub> : 0.40; SrO: 0.324; BaO: 0.16; ZrO <sub>2</sub> : 0.115; Nb <sub>2</sub> O <sub>5</sub> , Rb <sub>2</sub> O, MoO <sub>3</sub> , ZnO, In <sub>2</sub> O <sub>3</sub> , SnO <sub>2</sub> , RuO <sub>4</sub> <0.1
Specific surface area (BET method; m <sup>2</sup> g <sup>-1</sup> )	19.32
Particle size (microns)	250
<b>An azo dye of MO</b>	
Molecular formula	C <sub>14</sub> H <sub>14</sub> N <sub>3</sub> NaO <sub>3</sub> S
Other names	Sodium 4-[(4-dimethylamino)phenylazo] benzenesulfonate
Molecular weight (g/mol)	327.33
Azo type	Mono-azo
Chemical structure	

### 2.2 Methods

Natural clay was prepared by grinding and sieving the raw material through a 60 mesh screen to generate around 60 mesh or 250 microns of sieved clay. Then the element compositions of natural clay as the metal oxides formation, are represented from the XRF measurement as shown in Table 1. Eff. stationery and area were 13.0 mm and 132.7 mm<sup>2</sup> for the XRF measurement of natural clay utilizing Thermo Fisher Scientific's XRF with x-ray path: air.

Preparation of CuO/clay composite. Natural clay was intercalated using 0.1 M surfactant CMC and stirred at 60 °C for 24 h. Then the clay modification was separated from the solution and washed with demineralized water and ethanol until pH 7 was reached. The clay was dried at 60 °C for 3 hours [23]. The CuO/clay composite was prepared by the impregnation method [24], 5 g of clay was dispersed in 40 mL of distilled water and stirred. Then 5 g of CuSO<sub>4</sub>.5H<sub>2</sub>O was added to the mixture. The mixture was added 40 mL of ethanol 96% and stirred with a magnetic stirrer for 5 hours. It was filtered using a vacuum pump and the precipitate obtained was dried at 80 °C for 5 hours. Then the dry deposit was calcined at 400 °C for 5 hours. The CuO-clay composite was ground using a mortar and sieved through a 60 mesh sieve.

Characterization of CuO/clay composite. The phase of specimen was characterized by X-ray Diffraction (XRD, Shimadzu 7000) with CuKα radiation (λ = 1.5405 Å). The pore characteristic of specimen, including surface area, pore volume, and pore distribution was determined by adsorption N<sub>2</sub> using surface area analyzer (SAA, type Quantachrome Nova 4200e) with outgas time of 3 hours at a temperature of 250 °C and bath temperature of 273 K. The specific textural properties as the surface area and the pore volume were calculated using the Brunauer-Emmet-Teller (BET) by t-Plot method with the total pore volume was represented by the total adsorbed gas at relative pressure P/P<sub>0</sub> = 0.99, then for the pore distribution based on Barret-Joyner-Halenda (BJH) analysis. The microstructures of specimen were observed by Scanning Electron Microscopy (SEM, JEOL-6000PL), which qualitatively indicated grain size of 60 mesh, the quantitative analysis were also examined with energy dispersive analysis (EDX).

Determination of the mass optimum of composites, about 25 mg/L MO solution with a pH 4 (optimum condition of Liu et al. [25]) added with CuO/clay composites as much as 100, 200, 300, 400 and 500 mg. Then irradiated with UV lamp (Philips TUV 15W/G15 T8 with λ 280 nm) for 150 minutes. Furthermore, it was centrifuged at 7000 rpm for 15 minutes, then the absorbance was measured using Shimadzu UV-Vis spectrophotometer. The percentage of photodegradation calculated by Eq. (1).

$$\%D = \frac{C_0 - C}{C_0} \times 100\% \quad (1)$$

where %D is the percentage of photodegradation, C<sub>0</sub> is the initial concentration, and C is the concentration after

photodegradation process at the time  $t$ . It is also done to determine the optimum degradation time by using the optimum composite mass and variations in contact time of 60, 90, 120, 150, and 180 minutes.

### 3 Result and Discussion

#### 3.1 Analysis of SEM-EDX results

SEM analysis was used to investigate the changes of the surface morphology of clays and clays impregnated CuO. Based on Figure 1, it can be seen that the surface morphology of the clay is different from of the impregnated, CuO/clay. After the impregnation process by copper, the clay becomes more porous and expands.

This porous and swollen look is most likely caused by the impregnation process, which changes the surface charge of the particles, as well as the reduction of some amorphous phases that were initially connected to the clay. This is agreed with the previous study using copper nitrate salt as a CuO catalyst starter compound [24]. In addition, this is may be due to the strong immobilized CuO on the natural clay support [26]. The results obtained are also confirmed by the results of XRD analysis which will be discussed further. The same thing was also reported by Alakhras et al. [27] when titania ( $\text{TiO}_2$ ) was loaded with zeolite material. Besides, it also observed the surface morphology of CuO/clay composite is more uniform with spherical like structure while the natural clay have irregular blocky structure [28,29].

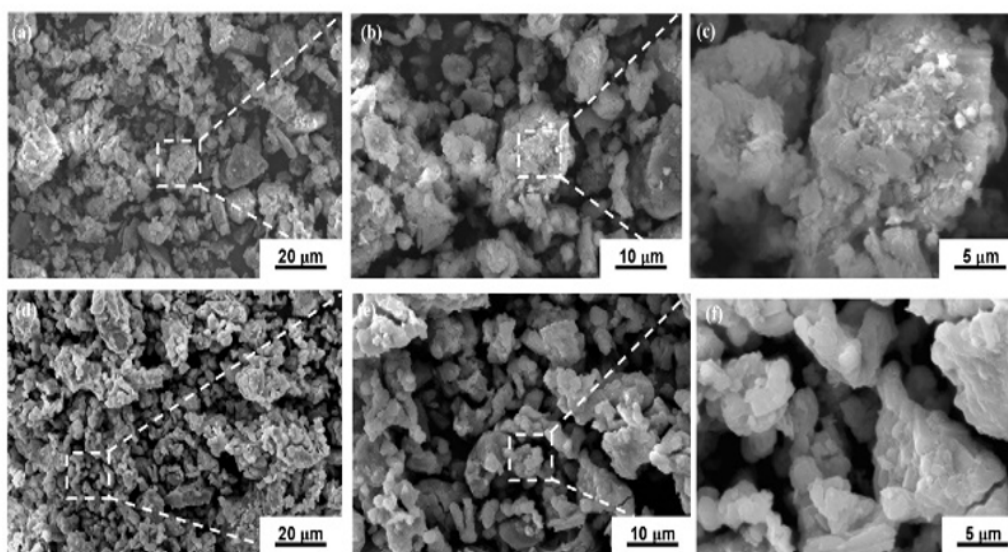


**Fig. 1.** The surface morphology of clay (a,b,c) and CuO/clay composite (d,e,f)

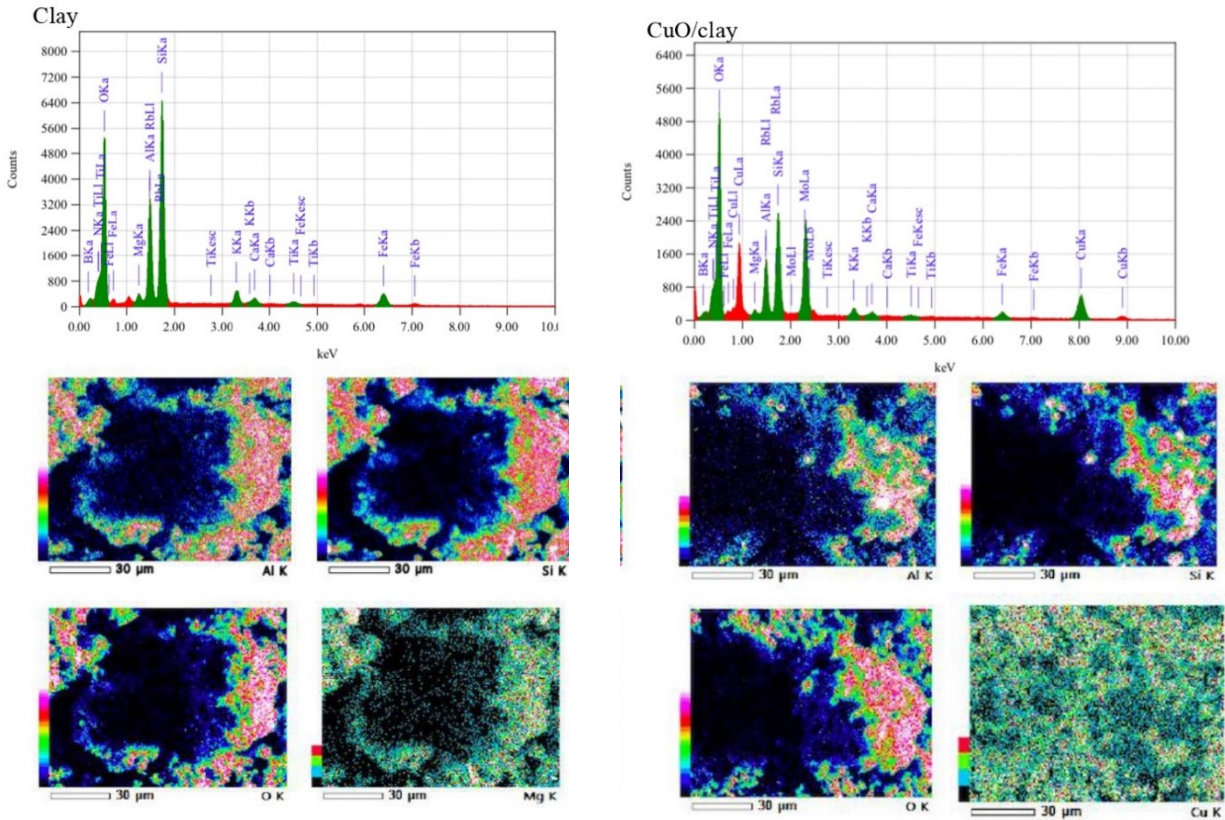
Elemental analysis of clay and CuO/clay composite was carried out using EDX microanalysis. The EDX results showed that neither Cu nor CuO compounds were detected in natural clay, and there were 21.34% and 26.72% respectively for Cu and CuO in clay impregnated catalyst samples. For investigate the distribution of CuO on the surface of clay, an EDS mapping analysis was also carried out on the samples. The results obtained show that the CuO catalyst spreads evenly on the supporting surface of the natural clay.

#### 3.2 Analysis of XRD results

The crystalline structure of samples was investigated by XRD, and the corresponding patterns are shown in Figure 3. The XRD patterns of clay was also presented

as a comparison condition before and after impregnation. The diffraction peaks for clay can be indexed by the characteristic  $2\theta = 19.91^\circ, 27.58^\circ, 27.85^\circ, 28.12^\circ, 29.89^\circ$  and  $35.34^\circ$ . The diffraction peak at  $2\theta 15.32^\circ$  with  $d_{001}$  attributed to the ordering of clay layers, related with the change of basal spacing [30]. Additionally, the reflection at  $19.91^\circ$  indicated that the montmorillonite phase of clay was detected [23].

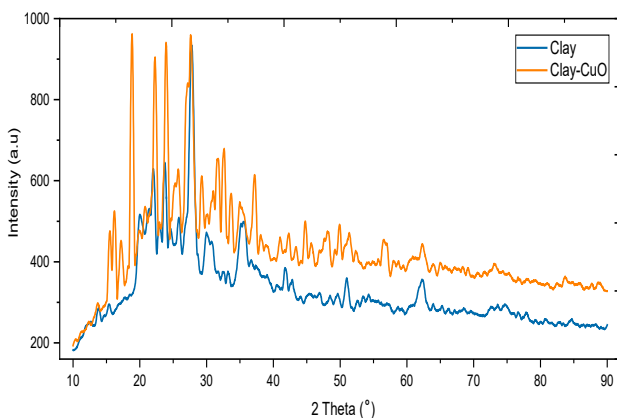
The diffraction patterns of CuO/clay indicated the reflection at  $2\theta = 35.29^\circ$  and  $38.50^\circ$  that correspond to the peaks of copper oxide and other reflection could be related to clay [23]. CuO's presence may be the cause of the CuO/clay peaks' broadening when compared to clay alone. The crystal parameter of CuO was detected with  $a=4.77 \text{ \AA}$ ,  $b=3.55 \text{ \AA}$ ,  $c=5.23 \text{ \AA}$  and the angle of  $\alpha = 90^\circ$ ,  $\beta = 98,59^\circ$ ,  $\gamma = 90^\circ$  (ICCD 01-080-0076). Therefore, the CuO/clay composite has a monoclinic crystal structure.



**Fig. 2.** The EDX Mapping of clay and CuO/clay

**Table 2** Analysis elemental of clay and CuO/clay composite

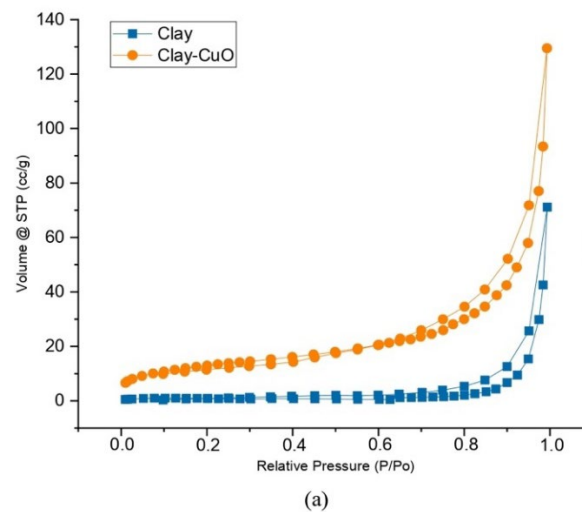
Element	Comp.	Mass (%) of element		Mass (%) of compounds	
		Clay	CuO/clay	CuO/clay	CuO/clay
O K	-	44.39	33.96	-	-
Al K	Al <sub>2</sub> O <sub>3</sub>	10.11	3.40	19.09	6.43
Si K	SiO <sub>2</sub>	20.53	6.46	43.92	13.82
Ca K	CaO	1.25	0.58	1.75	0.82
Ti K	TiO <sub>2</sub>	0.77	0.26	1.29	0.43
Fe K	FeO	8.11	2.41	10.43	3.10
B K	B <sub>2</sub> O <sub>3</sub>	3.10	1.62	9.97	5.21
N K	N	0.26	0.12	0.26	0.12
Mg K	MgO	0.72	0.29	1.19	0.48
Rb K	Rb <sub>2</sub> O	7.89	1.69	8.62	0.38
Cu	CuO	-	21.34	-	26.72



**Fig. 3.** The XRD patterns of clay and CuO/clay

### 3.3 Analysis of adsorption N<sub>2</sub> result

Adsorption of N<sub>2</sub> was carried out to identify the specific textural characteristics, and BET analysis was used to quantify the surface area and pore volume, BJH analysis was then used to determine the pore distribution are shown in Figure 4 and the corresponding in the Table 3. The isotherm of adsorption-desorption in Figure 4(a) shows that there are no noticeable hysteresis loops. The adsorption isotherms for clay and CuO/clay are close to type III, which indicates that the contact between the adsorbate and the adsorbed layer is larger than the interaction with the adsorbent surface, according to the Brunauer-Deming-Deming-Teller classification [31].



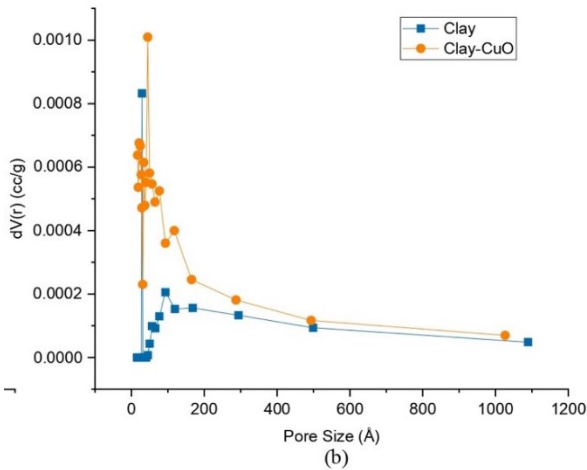


**Fig. 4.** (a) Isotherm of adsorption-desorption curves and (b) pore size distribution of samples

**Table 3** Pore characteristics of samples correspond from Figure 4

Samples	Surface Area (m <sup>2</sup> /g)			Volume @STP (cc/g)			Pore Distribution (Å)	
	<sup>a</sup> BET	<sup>b</sup> Micro	<sup>c</sup> Meso	<sup>d</sup> Total	<sup>e</sup> Micro	<sup>f</sup> Meso	Micro	Meso
Clay	31.65	2.01	2.08	0.23	0.026	0.204	84.3	25.2
CuO/clay	45.13	0.98	1.21	0.07	0.014	0.056	75.1	19.7

<sup>a</sup>BET surface area; <sup>b</sup>Micropore surface area evaluated by *t*-plot method; <sup>c</sup>Mesopore surface area calculated using  $S_{BET} - S_{micro}$ ; <sup>d</sup>Total pore volume at  $P/P_0 \sim 0.99$ ; <sup>e</sup>Micropore volume calculated by *t*-plot method; <sup>f</sup>Mesopore volume calculated using  $V_{total} - V_{micro}$ ; <sup>g</sup>Pore distribution based on BJH analysis.

### 3.4 Methyl Orange Photodegradation

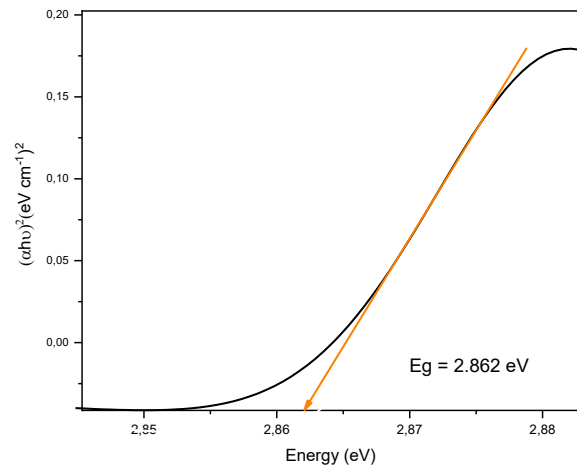
The ability of the material to produce radical ion for degrading organic compounds depends on the energy band gap ( $E_g$ ). The  $E_g$  in this study, analysis based on the UV-Vis spectra by applying Tauc's-plot to find relationship between the absorption coefficient ( $\alpha$ ) and the incident photon energy ( $\alpha h\nu$ ) as shown in Eq. (2).

$$\alpha h\nu = A (h\nu - E_g)^n \quad (2)$$

where  $\alpha$  is the absorption coefficient,  $h$  is Planck's constant ( $6.626 \times 10^{-34}$  J s),  $\nu$  is the frequency of light,  $c$  is the velocity of light ( $3 \times 10^8$  m/s), and  $\lambda$  is the wavelength of the spectra,  $n$  is 2 for indirect semiconductor and  $1/2$  for direct semiconductor.

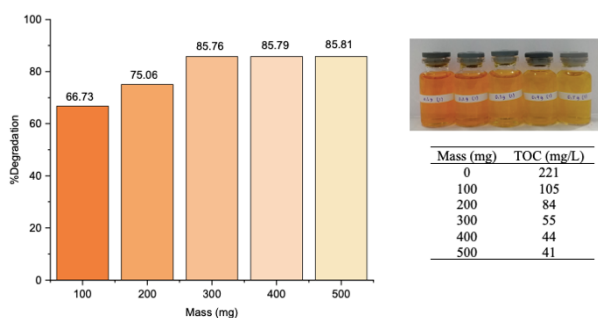
The optical band gap energy estimations of CuO/clay shown in Figure 5 and the value of band gap was determined to be 2.862 eV. The band gap value obtained is almost the same as the CuO nanoparticles that have been synthesized by the chemical precipitation method of 2.85 eV [33].

Table 3 shows that the impregnation of CuO catalyst against clay was successful, where the surface area of the sample increased and the pore volume decreased after impregnation of the catalyst. The same results was observed by previous studies that carried out impregnation of  $Fe_2O_3$  metal into porous ceramic support [17] and impregnation of Cu,Fe,Zn metal into HZSM-5 zeolite [32].



**Fig. 5.** Optical band gap energy estimations of CuO/clay composite

The resulting of CuO/clay composite was then applied to the MO dye photodegradation process in aqueous solution by examining the effect of composite mass and contact time on the percent degradation of MO dye as shown in Figure 6 and Figure 7, respectively.



**Fig. 6.** Effect of mass CuO/clay composite toward the photodegradation of MO dye

The effect of mass CuO/clay composite has been studied by applying the different amount (100, 200, 300, 400, 500 mg) of composite. The %degradation increase by increasing the amount of composite. It is clear from the results shown in Figure 6, the photodegradation increased rapidly with increase the amount of CuO/clay composite. This is due to the greater number of composites that interact with dyes, the greater amount of MO dyes that will be mineralized (TOC measures the concentration of C atoms as a whole and is not affected by the type of pollutant (aromatic or aliphatic). This is evidenced by the TOC value before the photodegradation process and after degradation decreased with increasing composite mass. This is agreed with the results of previous studies which explained that a decrease in TOC indicated progress in mineralization. This can be explained by the conversion of aromatic compounds into aliphatic compounds through ring-opening reactions [21].

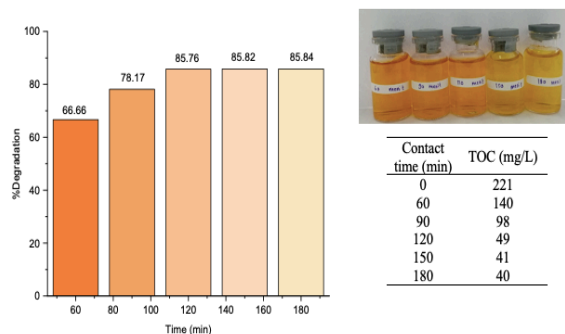


**Fig. 7.** Effect of contact time toward the photodegradation of MO dye using CuO/clay composite

The photodegradation of MO has been examined at various irradiation times when CuO has been present on the composite CuO/clay, as illustrated in Figure 7. With longer exposure times, MO was degraded more quickly through photocatalysis. At 180 minutes of exposure, the photodegradation was found to be 85.84%. This is brought on by a stronger interaction between the dye molecule and the photocatalyst surface as illumination time increases. As a result, the photocatalyst's photodegradation efficiency rise [34].

The findings of this study indicated that the optimum photodegradation efficiency of the composite for the removal of MO dye was 85.84% at the optimized composite mass of 500 mg with a contact time of 180 minutes. The degradation ability of CuO/clay composites against MO dyes is higher than the results of previous studies using TiO<sub>2</sub>/CuO composites [35].

However, the degradation ability of CuO/clay composites in this study was lower when compared to using ZnO/CuO nanocomposites [36]. This is presumably due to the low surface area of the resulting composite and the synthesized material has not yet led to the nanoscale, thus further studies are needed on particle size analysis of the resulting composite.

## 4 Conclusion

In the present work, the preparation and characterizations of CuO/clay composite for MO dye photodegradation were investigated. The results from SEM analysis revealed that there is a change in the surface morphology of the sample before and after impregnation, the clay becomes more porous and expands. XRD results show the CuO/clay composite has a monoclinic crystal structure. As for the sample surface area based on BET analysis using t-plot method, the surface area decreased after the CuO impregnated and the pore distribution using BJH analysis decrease, it indicates that CuO was successfully impregnated into the clay. The amount of CuO that was successfully impregnated into clay based on EDX analysis was 26.72%. The resulting composite was successfully used as a photocatalyst in the MO degradation, showing a degradation ability of 85.84% with a composite mass of 500 mg with a contact time of 180 minutes. This study is an important reference, significant for the treatment of dye wastewater, and could be informative for the sustainable development of future catalysts.

## References

1. M. A. Brown and S. C. De Vito, Critical Reviews in Environmental Science and Technology **23**, 249 (1993)
2. A. G. Acedo-Mendoza, A. Infantes-Molina, D. Vargas-Hernández, C. A. Chávez-Sánchez, E. Rodríguez-Castellón, and J. C. Tánori-Córdova, Materials Science in Semiconductor Processing **119**, (2020)
3. S. Sarkar, A. Banerjee, U. Halder, R. Biswas, and R. Bandopadhyay, Water Conservation Science and Engineering **2**, 121 (2017)
4. W. Konicki, M. Aleksandrak, D. Moszyński, and E. Mijowska, Journal of Colloid and Interface Science **496**, 188 (2017)
5. X. Jin, C. Wu, L. Fu, X. Tian, P. Wang, Y. Zhou, and J. Zuo, Journal of Environmental Sciences (China) **124**, 330 (2023)
6. A. C. Silva, J. S. Pic, G. L. Sant'Anna, and M. Dezotti, Journal of Hazardous Materials **169**, 965 (2009)
7. E. Guivarch, S. Trevin, C. Lahitte, and M. A. Oturan, Environmental Chemistry Letters **1**, 38 (2003)
8. A. Maroudas, P. K. Pandis, A. Chatzopoulou, L. R. Davellas, G. Sourkouni, and C. Argiris, Ultrasonics Sonochemistry **71**, 105367 (2021)

9. L. Karimi, S. Zohoori, and M. E. Yazdanshenas, *Journal of Saudi Chemical Society* **18**, 581 (2014)
10. X. Chen, Z. Wu, D. Liu, and Z. Gao, *Nanoscale Research Letters* **12**, 143 (2017)
11. Y. Zhang, F. Gao, B. Wanjala, Z. Li, G. Cernigliaro, and Z. Gu, *Applied Catalysis B: Environmental* **199**, 504 (2016)
12. T. N. J. I. Edison, R. Atchudan, M. G. Sethuraman, and Y. R. Lee, *Journal of Photochemistry and Photobiology B: Biology* **162**, 604 (2016)
13. M. Sudha, A. Saranya, G. Selvakumar, and N. Sivakumar, *International Journal of Current Microbiology and Applied Sciences* **3**, 670 (2018)
14. M. Ramesh, *Water Practice and Technology* **16**, 1078 (2021)
15. H. Yang, K. Dai, J. Zhang, and G. Dawson, *Chinese Journal of Catalysis* **43**, 2111 (2022)
16. M. Alhaddad, A. A. Ismail, Y. G. Alghamdi, N. D. Al-Khathami, and R. M. Mohamed, *Optical Materials* **131**, 112643 (2022)
17. S. E. Putri, D. E. Pratiwi, R. T. Tjahjanto, I. Andi, A. Rahman, I. Wulan, S. Ramadani, A. N. Ramadhani, and A. Fudholi, **17**, 503 (2022)
18. M. Amir, T. Fazal, J. Iqbal, A. A. Din, A. Ahmed, A. Ali, A. Razzaq, Z. Ali, M. S. U. Rehman, and Y.-K. Park, *Journal of Industrial and Engineering Chemistry* (2022)
19. A. Akbari, Z. Sabouri, H. A. Hosseini, A. Hashemzadeh, M. Khatami, and M. Darroudi, *Inorganic Chemistry Communications* **115**, 107867 (2020)
20. A. Nezamzadeh-Ejhieh and M. Karimi-Shamsabadi, *Chemical Engineering Journal* **228**, 631 (2013)
21. L. Hua, H. Ma, and L. Zhang, *Chemosphere* **90**, 143 (2013)
22. N. M. Mahmoodi, P. Rezaei, C. Ghotbei, and M. Kazemeini, *Fibers and Polymers* **17**, 1842 (2016)
23. S. Sohrabnezhad and M. E. Takas, *Journal of the Iranian Chemical Society* **16**, 45 (2019)
24. M. I. issi, Y. M. ah, A. La hrichi, M. C. ouch, and F. Z. uq, *International Journal of Innovative Research in Science, Engineering and Technology* **03**, 17359 (2014)
25. X. Liu, M. Liang, M. Liu, R. Su, M. Wang, W. Qi, and Z. He, *Nanoscale Research Letters* **11**, (2016)
26. O. Assila, M. Zouheir, K. Tanji, R. Haounati, F. Zerrouq, and A. Kherbeche, *Heliyon* **7**, e06069 (2021)
27. F. Alakhras, E. Alhajri, R. Haounati, H. Ouachtak, A. A. Addi, and T. A. Saleh, *Surfaces and Interfaces* **20**, 100611 (2020)
28. S. E. Putri, D. E. Pratiwi, R. T. Tjahjanto, D. Mardiana, and Subaer, *Journal of Chemical Technology and Metallurgy* **53**, 841 (2018)
29. S. Side and S. E. Putri, *Jurnal Akademika Kimia* **11**, 72 (2022)
30. H. Zhang, W. Wang, X. Wang, J. Xu, Y. Lu, and A. Wang, *Powder Technology* **396**, 456 (2022)
31. S. Brunauer, L. S. Deming, W. E. Deming, and E. Teller, *Journal of the American Chemical Society* **62**, 1723 (1940)
32. A. Alamdari and R. Karimzadeh, *Catalysts* **8**, (2018)
33. S. Sagadevan, K. Pal, and Z. Z. Chowdhury, *Journal of Materials Science: Materials in Electronics* **28**, 12591 (2017)
34. A. K and G. P, *Chemical Sciences Journal* **08**, (2017)
35. H. Koohestani and S. K. Sadrnezhad, *Desalination and Water Treatment* **57**, 22029 (2016)
36. M. Gerawork, *Optik* **216**, 164864 (2020)